Chapter 6

Bio-based poly(vinyline fluoride) hybrids for energy harvesting

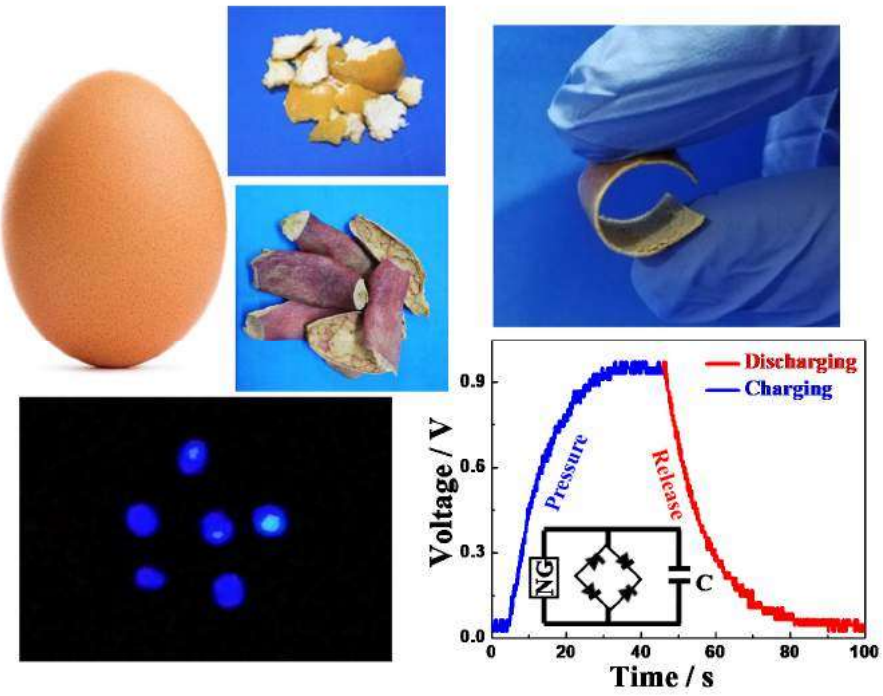

6.1. Introduction:

A self-powered system is the need of the day especially for real time biomedical health monitoring. Piezoelectric material based self-powered nanogenerators are of growing interest among researchers due to ease of application in biomedical devices and their suitability as flexible electronics [179, 180]. To use these nanogenerators in self powered biomedical devices, like in artificial cardiac pacemaker, the materials should be biocompatible. The biocompatible self-powered piezoelectric nanogenerators focus on common human body motion, especially, in in-vivo conditions and works for health monitoring and safety purpose [121, 181]. Naturally abundant piezoelectric materials are suitable for the designing of bio-medical nanogenerators or sensors which can operate without any adverse effect on the living systems. The natural piezoelectric materials like hydroxyapatite [182], collagen fibrils [183, 184], cellulose [81] and chitin [123] are the suitable choice for designing the biocompatible piezoelectric nanogenerator. On the other hand there are lots of bio-wastes which are causing the landfills and increasing the pollution at the same time. So, the green composites, derived from the natural materials or the bio-wastes are one of the best alternatives, as these contains natural fibers and these fibers have various benefits over glass fibers or carbon fibers like eco-friendliness, light weight, low cost, non-toxicity and biocompatibility along with their environment friendly behavior. By-products of the fruit processing industries are fruit wastes that consist of seed, core, peel and contain large amount of water and are in a wet and fermentable form. The idea of utilizing fruit waste especially peels started gaining popularity after the recent findings of easy processing and better biological activities than that of other parts of the fruits [185]. Extensive work has been going on in this area to search for possible substitute of the synthetic

fibers or materials for energy generation. A virus based piezoelectric nanogenerator has been fabricated but it shows very low power density [121]. The power generations by using prawn shell [123] and fish scale [122] as bio-waste are found to be of 0.76 and 1.14 $\mu W/cm^2$, respectively, while bio-waste onion skin is reported for electricity generation with meager power density of 1.7 $\mu W/cm^2$ [120].

In this chapter we have prepared PVDF hybrids with bio-wastes; eggshell membrane, orange peel and pomegranate peel for energy harvesting. The work is discussed in three parts: 1. PVDF hybrid with Eggshell membrane 2. PVDF hybrid with Orange peel, and 3. PVDF hybrid with Pomegranate peel.

Part-1

6.2. PVDF hybrid with Eggshell membrane

Here, we used the egg shell membrane (ESM) as one of the filler for preparing the hybrids of PVDF and two-dimensional layered silicate (nanoclay) for energy harvesting. ESM has many advantages as it is (i) inexpensive and readily available for use as industrial and household waste; (ii) it is non-toxic and environment friendly; (iii) it is composed of many proteins and amino acids having functional groups present on the surface which result in better functionalization capability and (iv) it has weak chemical bonding so it can readily be modified using carbonization and dissolution. Due to these advantages, ESM has been used in many fields, like chemical, electrical, environmental and biomedical engineering [186]. By adding ESM as second filler in the nanohybrid, the energy harvesting capability has been enhanced significantly with its biocompatible nature suitable for powering biomedical devices including implants.

6.2.1. Experimental:

The chicken eggs were procured from local market; the eggs are broken and the inner soft layer over the egg white *i.e.* egg shell membrane (ESM) is peeled out carefully. ESM is then dried in and crushed into fine powder to use as filler for hybrid preparation. Two types of hybrids are prepared using PVDF. One is two component (PVDF + nanoclay) and another is three component (PVDF + nanoclay + egg shell) system. The hybrids are prepared by solution route, as explained in **Chapter 2**. The hybrids of PVDF and ESM termed as P-ESM and hybrids of PVDF, clay and ESM termed as PC-ESM. The numeric term after shows the filler wt% in the hybrid.

Devices for energy harvesting prepared by same procedure explained in **Chapter 2**, but here aluminium foil is used to make sample conducting from both sides as the material is porous.

6.2.2. Results and discussion:

6.2.2.1. Structure of Eggshell membrane:

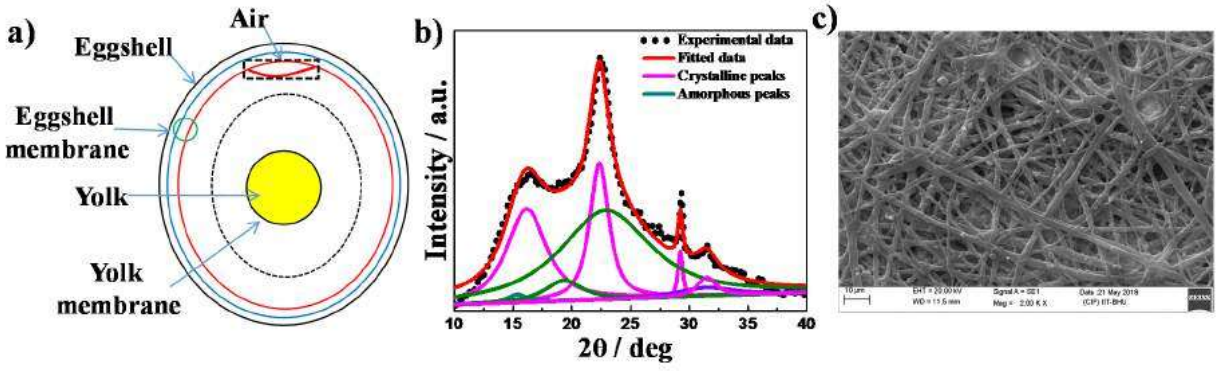

Figure 6.1: (a) Schematic of egg layers, (b) XRD and (c) SEM of eggshell membrane.

A hen's egg typically weighs almost 60 gm with a surface area of 53 cm^2. The egg shell membrane is one of the layers present in egg shell and has a total weight of 140 mg [187]. ESM is a fibrous structure which is situated between egg shell and the egg white (**Figure 6.1a**). The ESM fibers are 80-85% protein, of which ~10% is collagen (type I, V and X) and 70-75% are the secondary protein components including osteopontin, keratin, proteoglycans and glycoproteins [188-191]. The ESM and egg shell together contains more than 500 proteins, out of which the presence of 62 proteins is reported recently [192]. Wong et al. [193] reported the ration between collagen I and V is 100:1. The detail of proteins in egg shell matrix can be found in literature [194]. Each fiber of ESM has a collagen-rich core and a glycoprotein rich core [195]. The outer ESM fibers' core contains mainly type I collagen and inner fibers' core contain type I and V collagen [196]. Collagen type X is present in both the membranes [197]. The inner ESM is not calcified but the outer ESM fibers are partially mineralized [194, 198].

The X-ray diffraction (XRD) pattern of ESM is shown in **Figure 6.1b**. XRD pattern shows the crystalline nature of the ESM due to the presence of highly ordered collagen fibrils. The deconvolution of XRD pattern shows the crystalline phases present. The crystalline peaks suggest the presence of collagen, osteopontin, keratin, proteoglycans and glycoproteins [127, 199]. The amount of crystallinity through XRD deconvolution is around 40 %. The ESM is actually two shell membranes, mostly tightly bound together. The outer shell membrane has a thickness of 50-70 µm and has fibers of diameter 1 to 7 µm [200, 201]. The inner egg shell membrane has smaller diameter fibers of 0.1 to 0.3 µm range and has a thickness of 15 to 26 µm [200, 201]. **Figure 6.1c** show the scanning electron microscopy (SEM) images of egg shell membranes. A detailed study about these fibrous diameters has been done [186, 202].

We can see the 4-5 μm size pores around the fibers, which supports the fibrous nature of ESM. This highly ordered fibrous structure is responsible for the piezoelectric property of the ESM.

6.2.2.2. Induced structure and morphology

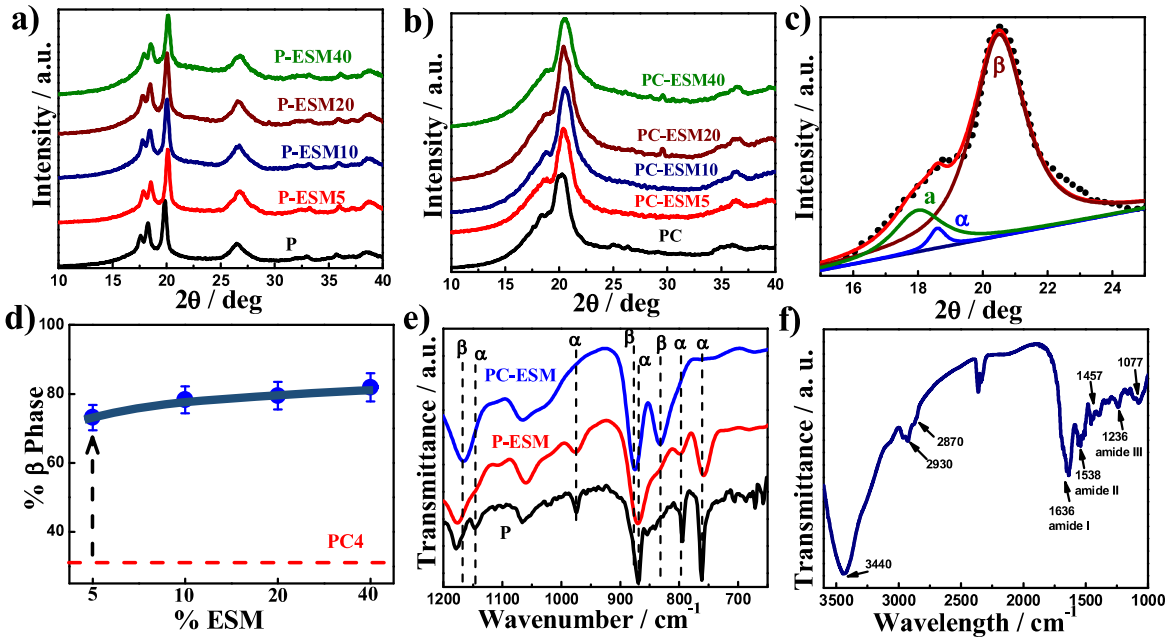

Figure 6.2: XRD pattern of (a) P-ESM hybrids, (b) PC-ESM hybrids with different ESM content, showing structural changes; (c) deconvolution of XRD pattern of PC-ESM40 for the calculation of phase fraction; (d) Plot of β-phase fraction with ESM content showing higher β–phase in PC-ESM. Dashed line indicate β-phase for PC and vertical arrow shows the jump in piezo-phase content; (e) FTIR spectra of Pure PVDF, P-ESM40 and PC-ESM40 hybrids indicating peak position of different phases and (f) FTIR spectra of eggshell membrane.

The gradual change over in structure in both hybrids is shown by X-ray diffraction (XRD) patterns of pure PVDF and its hybrids with ESM and nanoclay, with varying ESM content are shown. Pure α-phase peaks appear at 17.6° (100), 18.3° (020) and 19.9° (110) plane in pure PVDF [139] and the similar peak positions are observed in P-ESM hybrid (**Figure 6.2a**). On the other hand, crystalline β-phase peak at ~20.5° (corresponding to 200/110 planes) are

noticed in PC-ESM nanohybrid (**Figure 6.2b**). There is a clear change of phase from α to β in presence of nanoclay (nanoclay induced phase transformation) arising from the intimate interactions between nanoclay and PVDF chains [99] while ESM alone is unable to induce β-phase in the polymer. This is to mention that ESM shows ~40% crystalline phase (**Figure 6.1b**) and is known to be piezoelectric [127]. The amount of piezoelectric β–phase in hybrids is calculated through deconvolution of XRD peaks (**Figure 6.2c**) and the percentage β–phase fraction of various nanohybrids is shown in **Figure 6.2d** as a function of ESM content. PC shows a minimum piezoelectric β–phase (32%) while similar quantity of nanoclay induces large extent of β–phase in three component nanohybrids (82% β–phase using 40% ESM) with a gradual enhancement in piezoelectric phase with ESM content. This is worthy to mention that ESM alone cannot induce piezoelectricity in PVDF matrix while in presence of 2-D nanoclay huge piezoelectricity is induced in the matrix polymer. The structural alterations are also verified through FTIR spectroscopy by the presence of 836, 880 and 1167 cm^{-1} peaks assigned to β-phase in nanohybrids (PC, PC-ESM) against pure α-peaks at 761, 797, 869, 974 and 1146 cm^{-1} in PVDF and P-ESM (**Figure 6.2e**) [99, 203]. This is interesting to notice that α-phase peak intensity of pure PVDF has considerably decreased in P-ESM, though there is no β–phase peak, indicating reduced crystallinity in P-ESM presumably due to greater interaction between PVDF and ESM. **Figure 6.2f** shows the FTIR spectra of ESM, in which the peak at 3440 cm^{-1} corresponds to stretching mode of O-H and N-H groups. Peaks at 2932, 2869 cm^{-1} corresponds to stretching vibration of C-H bond present in the $=CH_2$ groups [204, 205]. In lower wavelength region, peaks at 1630 cm^{-1} (C=O), 1530 cm^{-1} (CN stretching/ NH bending modes) and 1234 cm^{-1} (CN stretching / NH bending modes) can be assigned to amide I, amide II and amide III vibrations of the glycoprotein, respectively

[206, 207]. The peaks at 1448, 1073 and 620 cm^{-1} is due to stretching modes of C=C, C-O and C-S bonds, respectively [206, 208, 209]. The ESM fibers are structurally stable due to their chemical bonding and crystallinity. As ESM have carbonyl, amide and –OH moieties, they are strongly associated with each other by Hydrogen bonding and dipoles present in the fibers facilitate the piezoelectric properties. So, the application of external force on the lattice crystal of the material changes its dipole arrangement, which have the key role in the piezoelectric effect [210]. The presence of ESM enhances the piezoelectric β–phase significantly in three component nanohybrids and therefore found suitable for energy harvesting application.

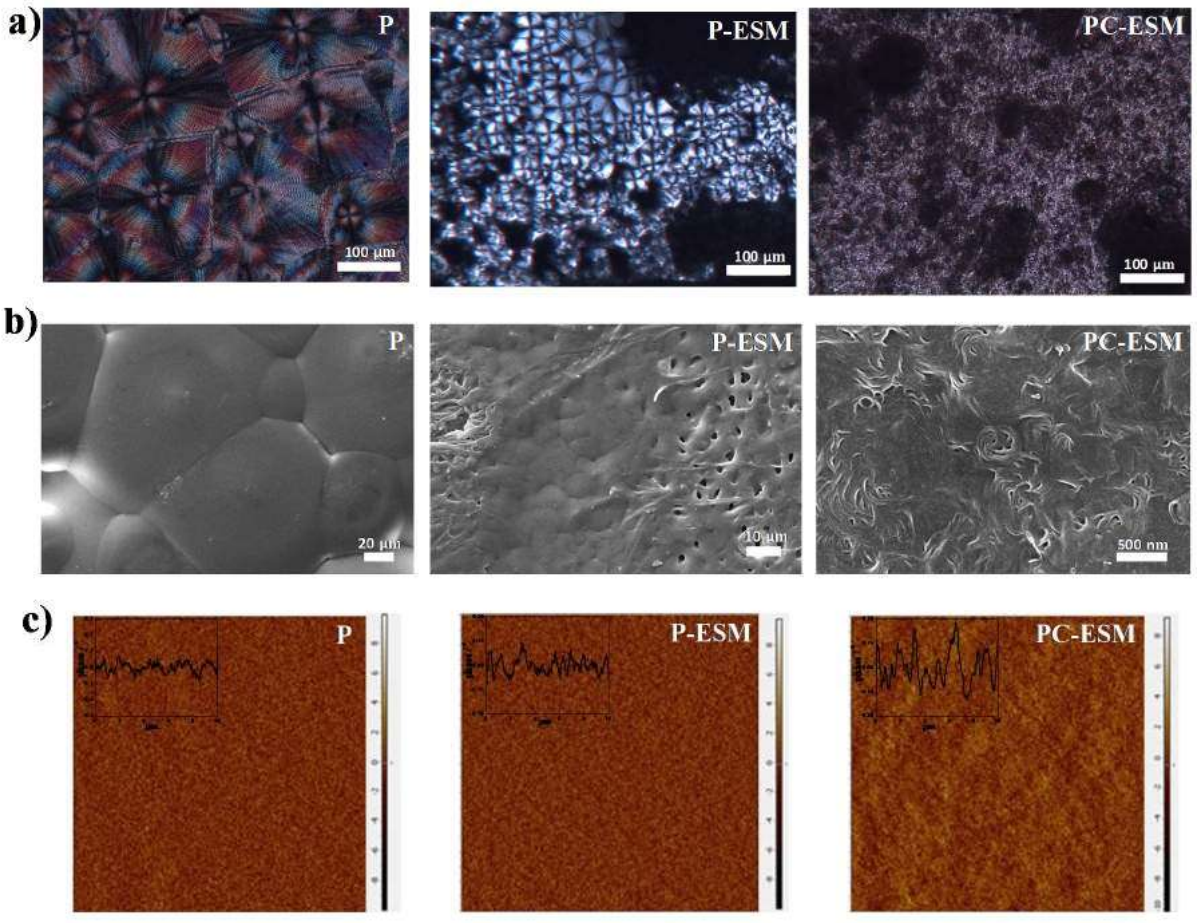

Figure 6.3: (a) Polarized optical images of indicated specimens showing spherulite in P and P-ESM and absence of spherulite in PC-ESM; (b) Scanning electron microscope images for pure PVDF, P-ESM and PC-ESM nanohybrids; (c) Piezo force microscopic images for pure PVDF, P-ESM40 and PC-ESM40 nanohybrids, inset shows the Phase profile of the specimens obtained from PFM images.

The structural change is often associated with the transformation of surface morphology. The polarized optical microscope images of pure PVDF and nanohybrids are shown in **Figure 6.3a**. Pure PVDF shows spherulitic pattern, indication of α-phase, with the average diameter of 200 μm while tiny spherulite (50 μm) along with fibrous morphology is observed in P-ESM in presence of 40 wt.% ESM. On contrary, mesh-like morphology is evident in PC-ESM which is a clear indication of β–phase in presence of nanoclay and ESM. This is to mention that fibrous morphology in observed in pure ESM (**Figure 6.1c**). Similar change of morphology is also observed through SEM where large and small spherulites are evident in P and P-ESM, respectively, while needle like β–phase morphology is obvious in PC-ESM in presence of nanoclay and ESM (**Figure 6.3b**). However, fibrous morphology of ESM along with β–nucleating 2-D layered silicate helps growing piezoelectric β–phase in large quantity. The enhancement in piezoelectric phase in three component nanohybrid is also be verified through piezo force microscopy. The change in the piezoresponse and phase dictate the presence of varying quantity of piezo phase domain upon the application of DC voltage of 10 V (**Figure 6.3c**). The line profiles corresponding to the phase angle of three different specimens clearly demonstrate the significant change in the phase behavior of PC-ESM as compared to pure PVDF or P-ESM hybrid (inset of PFM images). In this juncture, this is to mention that ESM (piezo filler) distributed in PVDF matrix cannot induce piezo phase in polymer matrix while it induce in large quantity of piezo phase in association with another 2-D nanoclay and convert most of the matrix into piezo phase commensurate with

the XRD and FTIR results leading to the development of two types of piezoelectric materials having piezo filler in non-piezo matrix (P-ESM) and piezo filler in piezo matrix (PC-ESM) and expected to exhibit very different energy harvesting behavior.

6.2.2.3. Energy harvesting using nanohybrid:

As the nanohybrid exhibits piezoelectric phase it should show the energy harvesting. We fabricate the nanogenerator for energy harvesting using suitable layer by layer assembly of active piezoelectric materials electrode and stable coating. **Figure 6.4a** shows the open circuit voltage (OCV) arising from the devices made of pure PVDF and nanohybrids with ESM and nanoclay plus ESM under finger tapping with a frequency of ~5 Hz. Three component nanohybrid (PC-ESM) exhibits the maximum peak to peak open circuit voltage of 56 V as compared to meager 4 and 33 V shown by the devices using pure PVDF and P-ESM, respectively. The estimated force from finger tapping is calculated to be around 40 kPa. The devices made of two component hybrids (P-ESM) show a strong ESM content variation under similar strain application using finger tapping (**Figure 6.4b**). OCV increase systematically with ESM content and achieve 35 V using 40 wt.% ESM. Interestingly, three component nanohybrids (PC-ESM) display higher OCVs as compared to two component hybrids (P-ESM) having similar ESM loading and shows 56 V using 40 wt.% ESM (**Figure 6.4c**) presumably due to higher piezoelectric β–phase in nanohybrid vis-à-vis P-ESM.

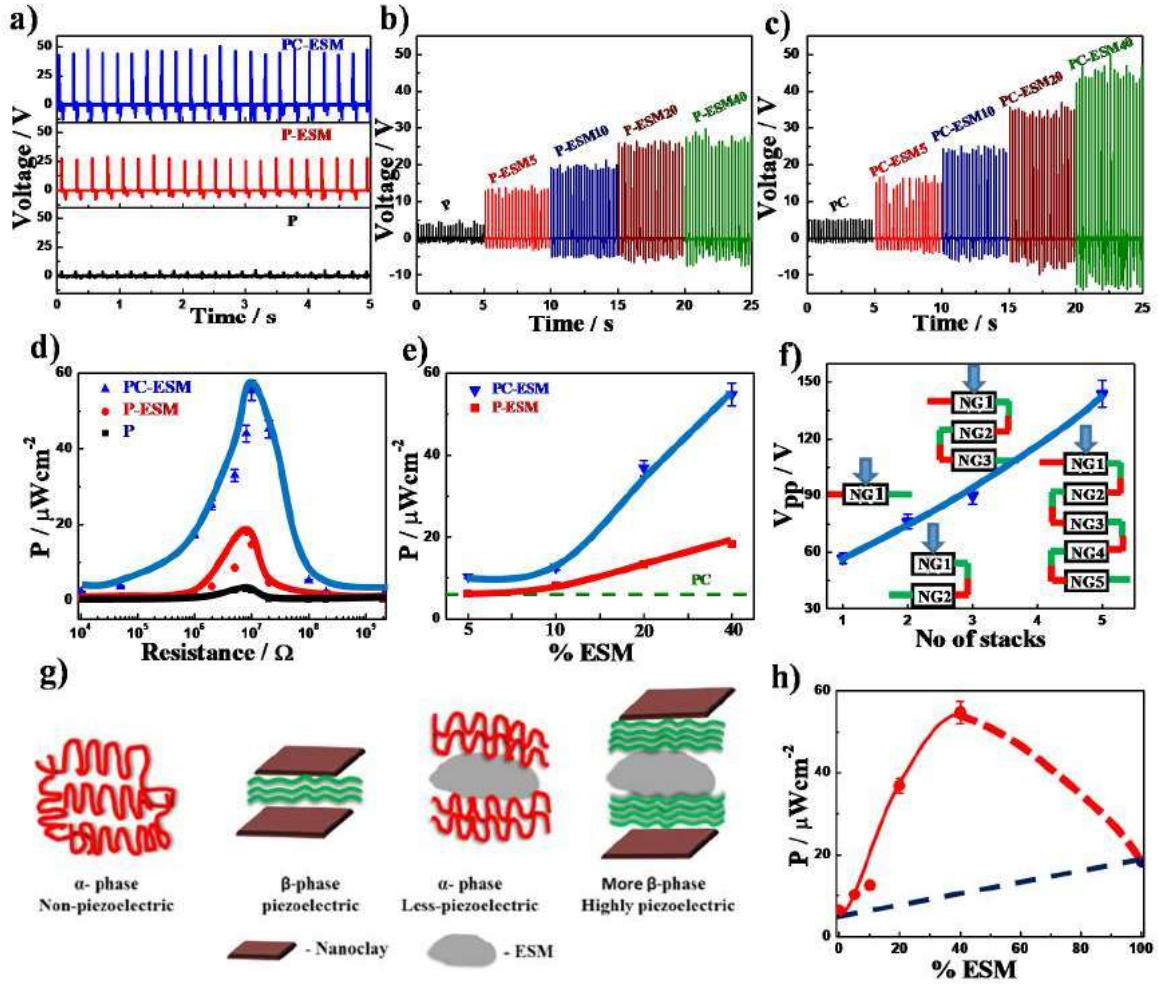

Figure 6.4: (a) Open circuit voltage from the devices using pure PVDF, P-ESM and PC-ESM nanohybrids with 40 wt.% ESM; Output OCVs from the devices fabricated using indicated ESM content in (b) P-ESM, (c) PC-ESM; (d) variation in power density with resistance in devices made from pure PVDF, P-ESM and PC-ESM nanohybrids with 40 wt.% ESM content; (e) Power density variation with ESM content from the devices made of P-ESM and PC-ESM nanohybrids. The dashed line indicate the power output value using device made of PC (PVDF and nanoclay); (f) Open circuit voltage from device fabricated with PC-ESM (40 wt.% ESM content) nanogenerator with increasing number of stacks as indicated; (g) Schematics showing local ordering in different nanohybrids demonstrating induced structure in presence of only ESM and combined effect of ESM and nanoclay; and (h) Power output from the device as a function of ESM content in PC-ESM nanohybrid demonstrating synergism of nanoclay and ESM which exhibit significantly high output.

Now, it is pertinent to quantify the performance of nanogenerator on the basis of output power density. The output power is calculated by measuring the voltage at different resistances, as the power depends on the external load applied on the system. The power density is calculated using the equation:

$$P=\frac{V^2}{R\times A},$$

where, V is the voltage across the resistance R and A is the area of the active device. Interestingly, the maximum power density of PC-ESM40 nanohybrid is 55 μW/cm^2 (**Figure 6.4d**). **Figure 6.4e** shows the enhancement in power density from the devices using both the nanohybrids with the increase of ESM content exhibiting systematic improvement of power density while PC-ESMs show significantly higher power output vis-à-vis P-ESM mainly because of higher piezoelectric content (β–phase) in presence of both ESM and nanoclay. The increase in power density of nanohybrids is significant as compared to only PVDF-nanoclay composite (indicated by dashed line in the **Figure 6.4e**).To check the commercial viability of the device, multiple devices (2, 3 and 5 units) are assembled in series and their corresponding output voltages are presented in **Figure 6.4f** under similar finger tapping as before showing gradual increase of output voltage with increasing number of stacks with very high (144 V) output and 100 μW.cm^{-2} for 5 units stack device in series. Thus, the output voltage of the device can be amplified to the desired value by assembling the multiple devices which makes it more feasible for use in large scale industrial applications. The possible working mechanism of the voltage generation is explained by considering the physical changes (rotation of dipole) upon application of mechanical stress in compression and release mode. In PVDF and nanoclay hybrid (PC), the piezoelectricity is explained through epitaxial crystallization of the PVDF on the surface of 2-D nanoclay, which leads to the transformation

of its α-phase into electroactive β-phase and the extent of conversion dictate the piezoelectric phase. The ESM has porous structure which makes it soft and flexible and eventually it leads to more displacement than the normal compact structure under fixed load giving rise to high piezoelectricity in ESM [107]. The piezoelectricity in ESM is due to the combined effect of the collagen and the proteins. The polarization and piezoelectricity in type I collagen fibrils has been established due to the existence of N and C terminal telopeptides and C6 symmetry in the crystalline chain. External compressive stress on the oriented collagen structure induces high internal friction among the hydrogen bonded α-helices [211]. So, the deformation of the triple helical structure helps creating the dipole moments in ESM under stress. The similar mechanisms are explained in M13 bacteriophage [121], fish scale [122] and fish swimming bladder [124]. ESM has many collagen micro-fibrils which generate the electric dipole moment on the application of mechanical stress [211]. Hence, under applied stress the charges develop on top and bottom of ESM due to the breaking of symmetry present in the collagen moiety [184, 212]. The enhancement of the piezoelectric response in nanohybrid is directly related to the mutual electromechanical interactions among the fibers (needle like β–phase in matrix and ESM fibril) under external applied stress [184, 212]. There are different types of proteins in ESM and, hence, there is a possibility of interconnection between them either through hydrogen bonding or Van der Walls interactions which disrupt under mechanical stress leading to enhanced piezoelectricity in nanohybrid. Apart from this, the porosity of ESM plays an important role as the porous structure gets more displacement than the compact one under similar applied stress [107, 213]. However, the potential difference, caused by the orientation of electric dipole, results in electron flow from one to another direction while the electrons flow in the reverse direction

upon releasing the stress causing alternating current in the circuit [161]. Based on the varying nature of interactions in various hybrids / nanohybrids, the location and crystallization are presented in the form of a cartoon in **Figure 6.4g**. Pure PVDF crystallizes only in α–phase and does not show any piezoelectricity while nanoclay induce β–phase in PVDF (PC) whose overall crystallinity is less and thereby exhibit meager piezoelectricity. The introduction of electroactive ESM in pure PVDF (P-ESM; piezo phase in non-piezo matrix) shows α–phase PVDF matrix where piezo filler is dispersed and this system exhibit moderately high piezoelectricity having higher ESM content hybrid. On the other hand, good interactive three component systems (PC-ESM) induce β–phase in PVDF matrix along with piezo filler makes a near ideal system where the whole materials exhibit piezo phase (except small amorphous phase present in the system) showing layered orientation of three different components namely β–phase on the surface of 2-D nanoclay along with a layer of ESM. Now, it is apparent that ESM increase the piezoelectricity to a limited extent only while nanoclay and ESM enhances to a much greater value of piezoelectricity and subsequent power generation raising a possibility of synergism. Output power from the devices has been plotted as a function of ESM content in PC-ESM showing strong synergism (significantly above the values predicted by linear mixture rule as shown by the dotted line in the figure) (**Figure 6.4h*)***. This synergism is insignificant in P-ESM presumably due to less interaction between PVDF and ESM.

6.2.2.4. Practical applications of nanogenerator:

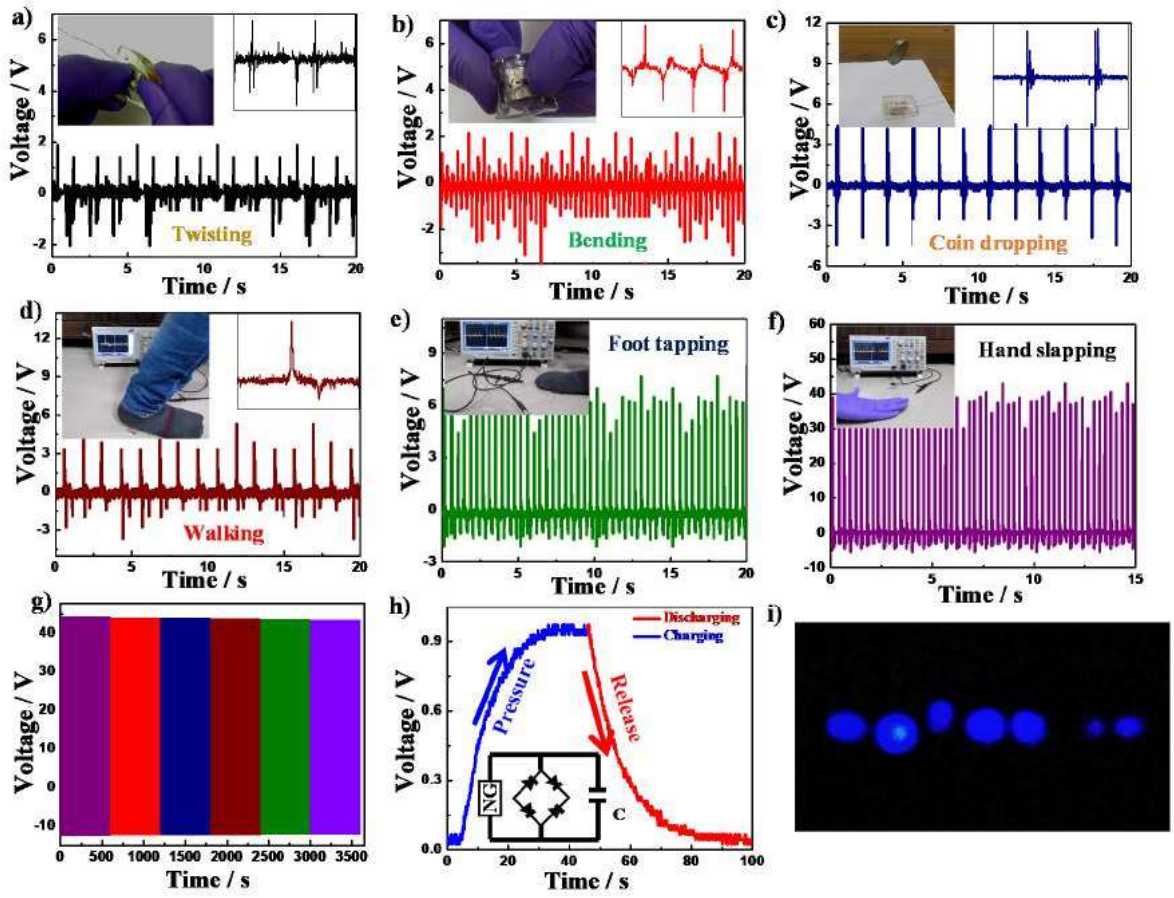

Figure 6.5: Demonstration of practical applications of the nanogenerator to harvest energy by applying normal human movements *e.g.*(a) Twisting; (b) Bending; (c) coin dropping; (d) Walking; (e) Foot tapping; and (f) Hand slapping; (g) Mechanical and durability test of the device after obtaining the device performance for sufficiently long time showing almost similar output voltage; and (h) The ability of output power from the device to charge a capacitor followed by discharging kinetics using the device made of PC-ESM40 (i) the LEDs glowing on the finger tapping.

In the preceding section, very high power generation is demonstrated using the three component nanohybrid applying finger tapping method. The harvesting ability of the devices may also be verified with different human activities as waste mechanical energy sources to understand the efficacy of the energy harvesting. **Figure 6.5a** shows the voltage output upon

twisting the nanogenerator (PC-ESM) which produces peak to peak output voltage of ~4V. The inset images show the force application mode and zooming of the output voltage. On bending (**Figure 6.5b**) and coin dropping (**Figure 6.5c**) (INR rupee 5 coin) the device produces ~5.6 and 8V, respectively, although the weight of the coin is less but the impact of the free falling coin is more and justify the higher output. For more realistic application, the output voltage from nanogenerator on walking is shown in **Figure 6.5d** as ~9.5 V, and on foot tapping the output voltage is measured to be ~10 V (**Figure 6.5e**) which can also light up LEDs. Hand slapping method is found to be more effective with the output voltage of ~50 V, significantly higher than other modes primarily due to greater impact and higher contact area (**Figure 6.5f**). However, various body motions can also generate significant voltage for harvesting the energy. The mechanical stability and durability test of the device is shown in **Figure 6.5g**, which clearly demonstrates good performance of the device even after repeated use. Now, it is pertinent to understand whether the device is able to store charge in capacitor. The device is attached to the capacitor (1 μF) through rectifier circuit and also connected to a digital oscilloscope to read the corresponding charging and discharging voltages from the device. Hand tapping method demonstrates the charging of capacitor and reaches a plateau followed by discharging (**Figure 6.5h**). The response time for charging and discharging phenomena are found to be 30 and 35 s, respectively. However, the nanogenerator made of bio-waste and nanoparticle embedded in PVDF is able to produce sufficient energy which can be stored and utilize later demonstrating the efficacy of the bio-inspired device for energy harvesting purpose. Using the nanogenerator LEDs can be lighten up as shown in **Figure 6.5i**. From these results it is clear that our bio-based piezoelectric nanogenerator is efficient for realistic applications.

Part-2

6.3. PVDF hybrid with Orange peel

The fruit wastes are rich in fibers, proteins, oils and flavonoids and orange peel is a good example of it. Flavonoids, present in the orange waste at different stages of the industrial processing, are found to be abundant in peels than that in juice, revealing their great industrial potential [214]. The chemical and antioxidant properties [215] of citrus peel indicate their good source of natural bioactive compounds including blended diesel as alternative fuel [216]. In the energy sector, the orange peel waste has been used in microbial fuel cell for bioelectricity production, without any chemical pretreatment or the addition of extra media showing output voltage and current density of 0.59 V and 847±18.4 mA/m^2, respectively [217]. The composition of orange peel on dry basis is shown in Table 6.1, which shows it has cellulose, hemicellulose, lignin, pectin and other proteins, which are responsible for its piezoelectricity [218]. Here, for the first time, orange peel has been used in the form of polymer hybrid as a potential candidate for energy harvesting novel material and a device has been fabricated for energy harvesting from various body movements and lighting the LEDs from door sliding.

Table 6.1: Composition of orange peel (on percent dry basis) [219].

Compound	Percentage
Soluble sugars	16.9
Starch	3.75
Cellulose	9.21
Hemicellulose	10.5
Lignin	0.84
Pectins	42.5

Ashes	3.50
Fats	1.95
Protein	6.50
Other compounds	4.35

6.3.1. Experimental:

Orange peels are dried and crushed into fine powder and used as filler for hybrid preparation. The hybrid of Poly(vinylidene fluoride) and orange peel powder is prepared by solution method discussed in **Chapter 2**. The weight fraction of 10, 20 and 40% is taken for preparation of hybrids. Pure PVDF, orange peel and nanohybrid are thereby abbreviated as P, OR and P-OR, respectively. The numeric terms after P-OR indicate the percentage of filler in the hybrid. For energy harvesting the device is prepared by conducting coating and electrode attachment as discussed in **Chapter 2**.

6.3.2. Results and discussion:

6.3.2.1. Structure and morphology:

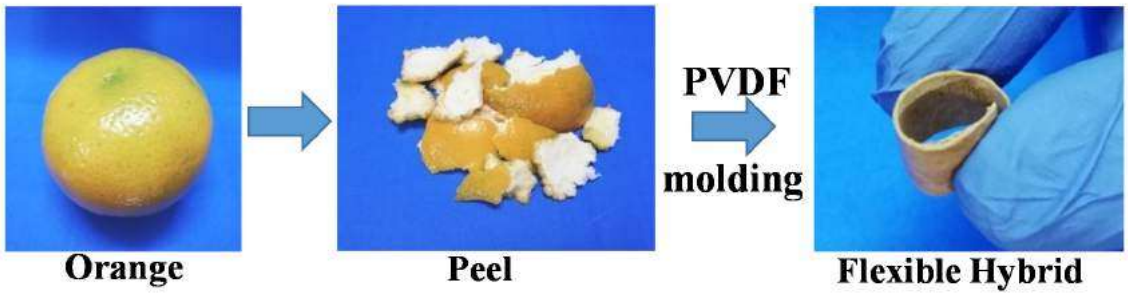

Figure 6.6: Photographic images of orange peel and synthesized hybrid showing its high flexibility and mechanical stability.

For energy Harvesting using orange peel the PVDF-Peel hybrid is prepared and the steps are shown in **Figure 6.6**, which shows highly flexible and mechanically stable nature of the hybrid. X-ray diffraction patterns of PVDF (P) and hybrid (P-OR) clearly demonstrate the structural changeover to electroactive β/γ-phase (2θ ~20.3° (200/110), 18.6° (020)) in hybrid from the α-phase (2θ ~17.6° (100), 18.3° (020) and 19.9° (110)) of pure PVDF (**Figure 6.7a**) [99, 139, 203]. The semicrystalline nature of pure peel is presented in inset of **Figure 6.7a**. The extent of electroactive phases (β and γ)in the hybrids is calculated through the deconvolution of XRD patterns (**Figure 6.7b**) and is found to be ~70% in the hybrid (**Figure 6.7c**). The induced piezoelectricity in PVDF is primarily due to the presence of peel and overall piezoelectricity of the hybrid is much higher considering the piezo-phase of orange peel filler.

The composition of orange peel is also confirmed through FTIR studies (**Figure 6.7d**). In which most of the bands are those observed in cellulose, hemicelluloses and lignin FTIR spectra [220, 221]. The peaks at 3298, 3318, 3275 and 3292 cm^{-1} are due to -OH vibrations form alcoholic and pectic acid components. The peaks at 2924 and 2920 cm^{-1} is due to the C-H asymmetric stretching vibration of aliphatic structures [220]. Peaks at 1732 and 1717 cm^{-1} can be assigned to C=O stretching of carboxylic acids. It should be noted that the C=O stretching vibration corresponds to aldehydes and observed in 1735 cm^{-1} range [222, 223]. Peaks at 1605, 1597 and 1612 cm^{-1} are stretching vibration of C=C. The peaks at 1413, 1273, 1368 and 1328 cm^{-1} is for vibrations of aliphatic chains $–CH_2-$ and $–CH_3-$, which form the basic structure of the cellulose materials. The 1054, 1011 and 1026 cm^{-1} signals can be attributed to C-O-H and C-O-R (alcohol or esters) vibrations [224, 225]. The FTIR of pure PVDF and hybrids shown in **Figure 6.7e**, which shows that the α-phase peaks at 760, 796,

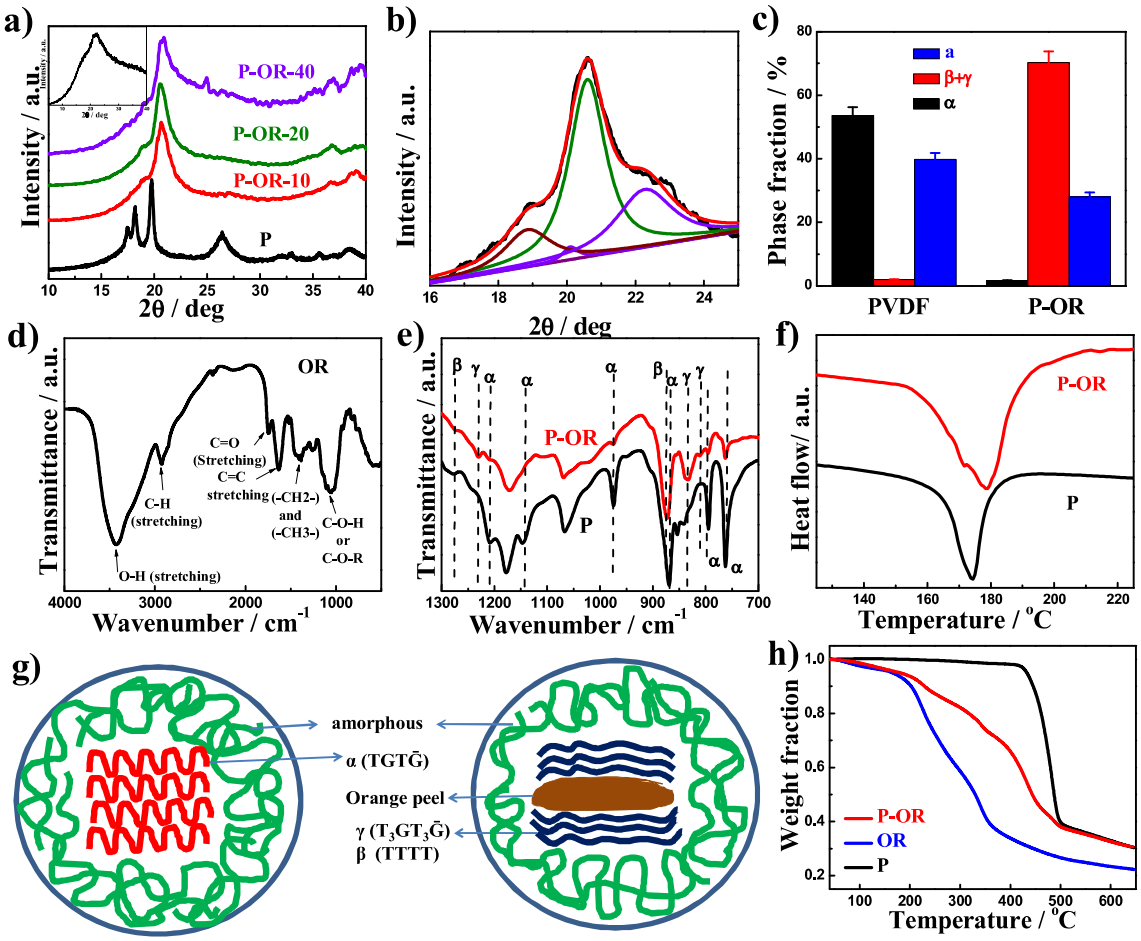

Figure 6.7: (a) XRD patterns of PVDF and hybrid showing different crystalline planes, inset shows the XRD plot of pure orange peel; (b) deconvolution of XRD plot (c) percentage of different phases present in PVDF and hybrid P-OR40 (d) FTIR spectra of orange peel (e) FTIR spectra of PVDF and hybrid indicating peaks corresponding to different phases; (f) melting thermograms of PVDF and hybrid. Dashed lines indicate the deconvoluted patterns of β– and γ–phase of hybrid; (g) Schematic for crystallization of PVDF at the interface of orange peel and (h) thermal stability of PVDF, peel and hybrid as measured through thermogravimetric studies.

866, 975, and 1210 cm^{-1} is evident in pure PVDF [140, 158] while characteristic β-phase peak at 1275 cm^{-1} and γ-phase peak at 1232 cm^{-1} are prominent in hybrid in addition to combined β- and γ-phase peaks at 810, 840 and 878 cm^{-1} [46, 226]. The phase alteration is also reflected in melting behavior as evident from single melting temperature of 173.5°C in pure PVDF

against double melting at 171°C (due to lower melting β-phase) and 179°C (arises from high melting γ-phase) (**Figure 6.7f**) following order of melting as γ>α>β [136]. The structural change in hybrid is due to crystallization of PVDF on the surface of orange peel which leads to induction of β and γ-phase (**Figure 6.7g**). The PVDF crystallizes in the mixed β and γ-phase as clear from the XRD, FTIR and DSC data. At the interface, there is mixed β and γ-phase and above that when the interaction becomes weak, there is α-phase, which is surrounded by amorphous phase. The thermal study of orange peel, pure PVDF and hybrid is shown in **Figure 6.7h**. The thermal stability of hybrid has been shown be up to 150°C and reduction of degradation temperature appears due to excess water molecules, cellulose and lignin present in orange peel [219]. The thermal degradation curve of pure orange peel is obtained as a sum of the degradation curves of its constituents. The degradation of OP occurs in three steps. The initial mass loss (~7%) below 100°C is due to release of weakly bonded water molecules or physically absorbed water molecules. We can see the degradation occurs in steps associated with its components (hemicelluloses, cellulose and lignin). According to previous studies, the polymeric composition of lingo-cellulosic material is complex and at least two mechanisms coexist during pyrolysis process [225, 227]. The first one (at lower temperature) corresponds to the pyrolysis and heterogeneous oxidation, hereas the second one is attributed to the combustion of char. The sample mass decreases continuously between room temperature and 590°C, which is related to the dehydration process and thermal degradation of the OP.

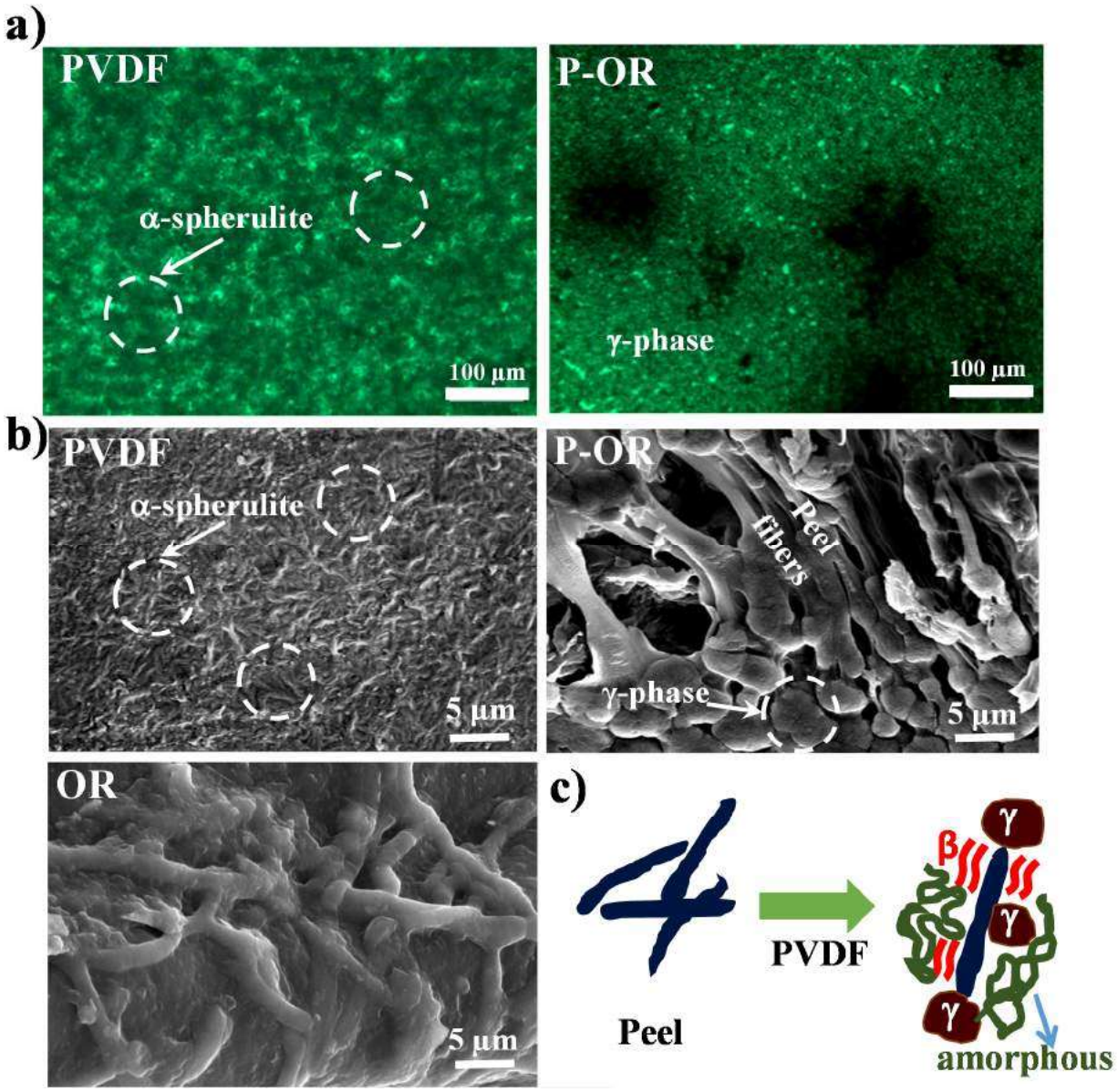

Figure 6.8: (a) Polarized optical microscopic images of as cast PVDF and hybrid (P-OR-40) thin films indicating various phase of crystallites; (b) Surface morphology of PVDF, hybrid and orange peel showing different crystallites and fiber as observed through SEM; and (c) schematic of PVDF crystallization at the edge of peel fibers demonstrating the appearance of electroactive induced phases in polymer matrix.

Solution cast thin film of PVDF shows α-phase spherulitic pattern as observed through polarized optical microscope while γ-phase is evident in hybrid (P-OR) as further confirmed

from its higher melting (180°C) under slow scan (**Figure 6.8a**) [99, 154]. The complete change in morphological patterns with temperature both for PVDF and P-OR is presented in **Figure 6.9** showing the respective phase melting at two different temperature. For pure PVDF there is partial change in morphology at 175 °C and full change at 177 °C and there is no change above this temperature, while for hybrid at 178 °C there are partial changes, while complete changes is at 180 °C and above this temperature there is no change.

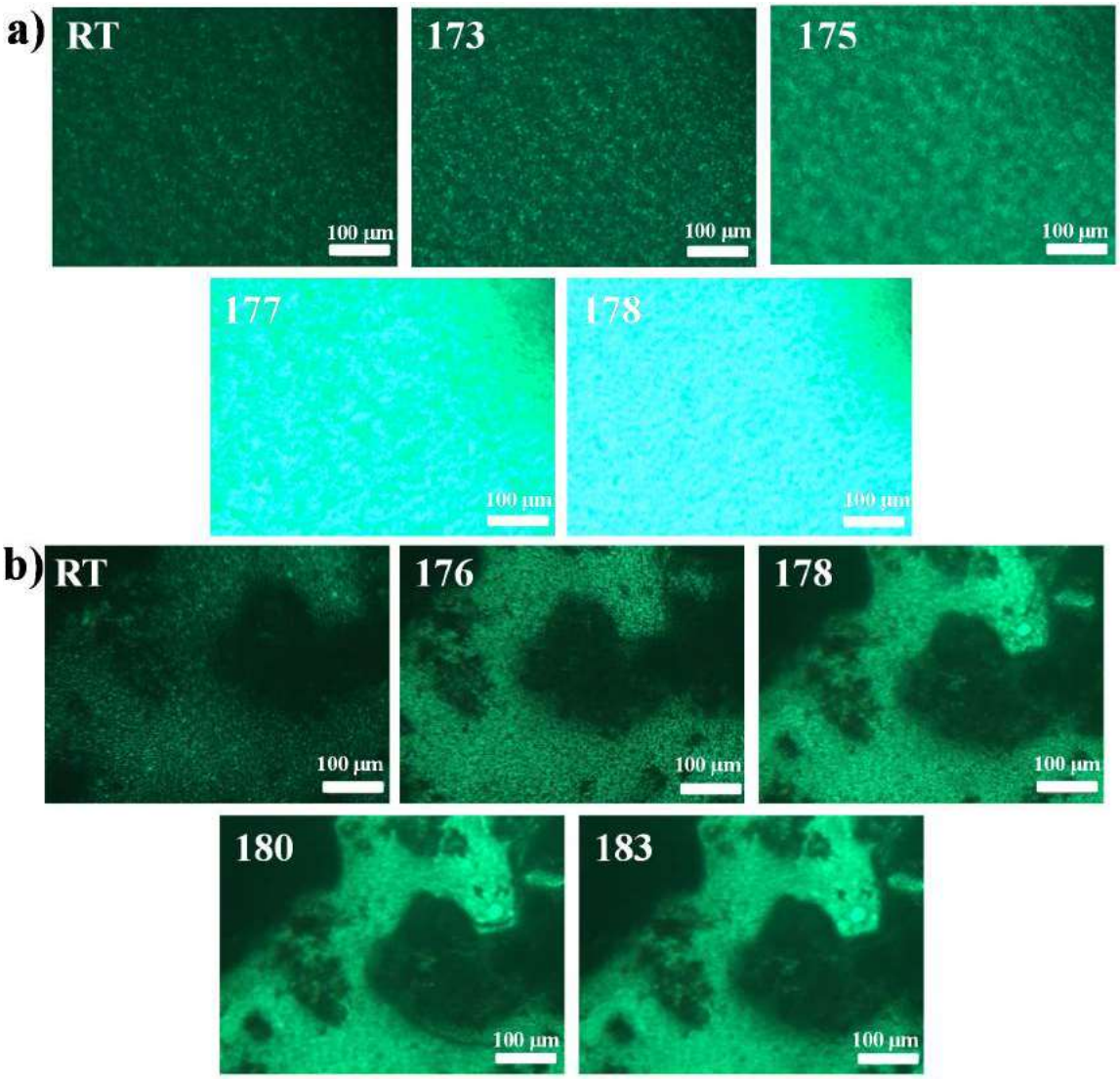

Figure 6.9: Polarized optical Microscopy images of a) PVDF and b) hybrid with changing temperature.

Surface morphology as observed through scanning electron microscope indicates the presence of α-spherulites in pure PVDF as opposed to fibrous morphology due to orange peel along with smaller and bright γ-spherulites in P-OR (**Figure 6.8b**). The appearance of fiber in the hybrid is due to the presence of peel as the surface morphology of orange peel clearly exhibits the fibrous pattern. Now, the induced crystallization of electroactive β/γ-phase is revealed and polymer chains can crystallize at the periphery of orange peel fiber both in all-trans needle-like β-phase, mostly at the side wall of the fiber, and tiny bright γ-spherulite, mostly at the edge of fiber, leading to thicker and dumble-like fiber in the hybrid. This induced piezoelectric crystallization has been shown in the form of a cartoon where thicker and dumble-like fiber is shown in the hybrid which directly corresponds to the thin fiber structure of pure orange peel and thick dumble-shape morphology of the hybrid (**Figure 6.8c**).

6.3.2.2. Energy harvesting and useful applications:

The energy harvesting performances have been studied using the devices which exhibit open circuit voltages (OCV) of 3, 58, 70 and 90 V from P, P-OR-10, P-OR-20 and P-OR-40,respectively, indicating higher voltage output from greater peel content hybrid against meager voltage output from pure PVDF being non-piezoelectric (**Figure 6.10a**). The power density, calculated from the equation $P = \frac{V^2}{RA}$, is found to be as high as 135 μW/cm^2 under

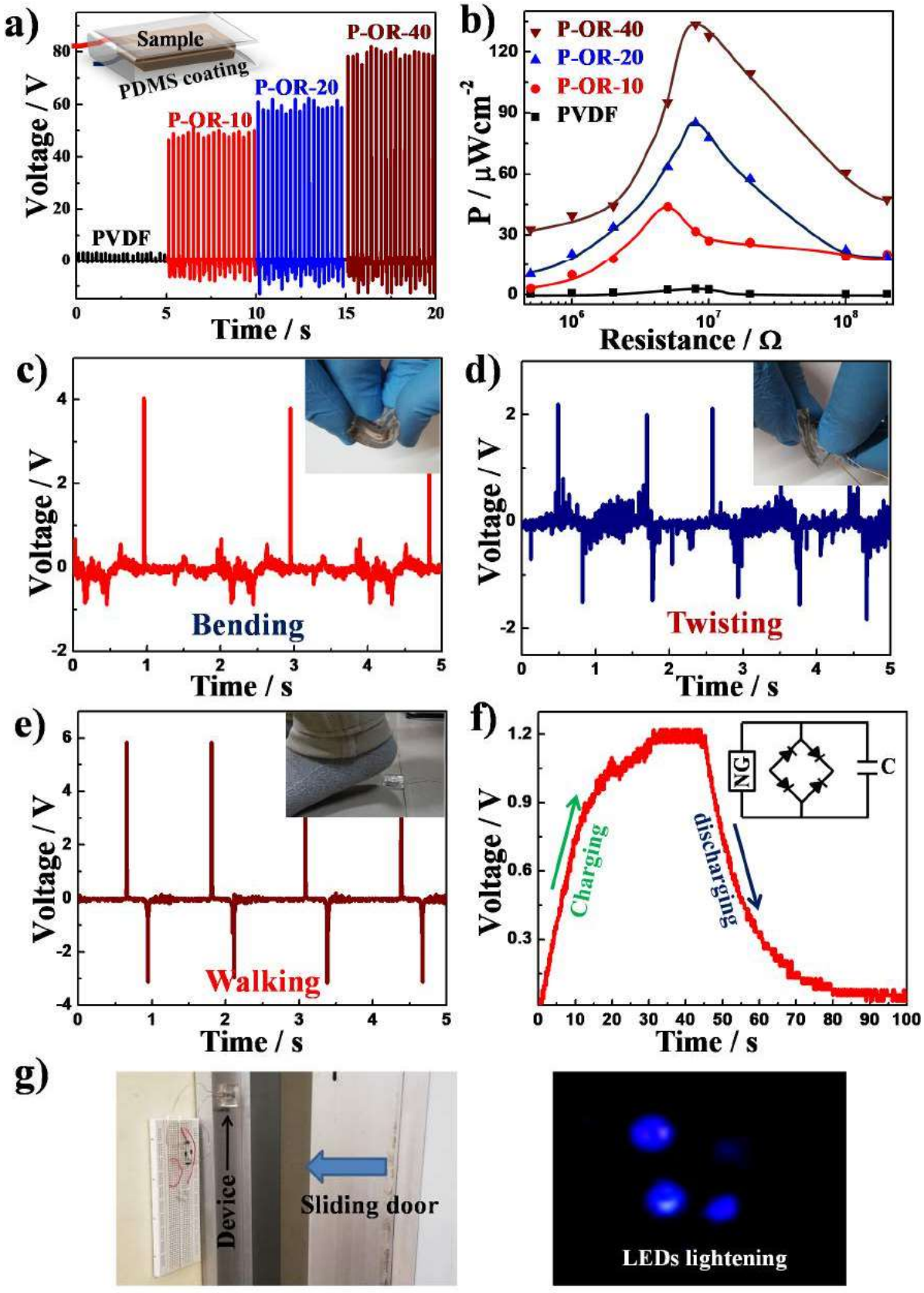
a)
Sample
PDMS coating
P-OR-40
P-OR-20
P-OR-10
PVDF
Voltage / V
Time / s
b)
P-OR-40
P-OR-20
P-OR-10
PVDF
P / μWcm-2
Resistance / Ω
c)
Bending
Voltage / V
Time / s
d)
Twisting
Voltage / V
Time / s
e)
Walking
Voltage / V
Time / s
f)
Charging
discharging
NG
C
Voltage / V
Time / s
g)
Device
Sliding door
LEDs lightening

Figure 6.10: (a) Open circuit voltage obtained from devices made of indicated hybrids or pure PVDF (inset shows the schematic of prepared device). The numbers after P-OR represent the amount of orange peel (w/w); (b) output power from the devices under varying applied resistance; Voltage generation from the device under different body movements (c) bending, (d) twisting and (e) walking on the device. Inset figures show the type of loading on the device; (f) charging and discharging nature of a capacitor from the energy produced by the device under finger tapping; (g) lightening of LEDs from energy produced by the device from household door sliding.

varying applied resistance (**Figure 6.10b**). Device made of pure orange peel generates meager 30 V (OCV) and 25 $\mu W/cm^2$ power, very low as compared to hybrid, raising a synergistic effect in hybrid as revealed through induced piezoelectric phase in polymer matrix (*cf* **Figure 6.7**) in presence of tiny peel powder as filler. The bio-waste (orange peel composed of many bio-polymers like cellulose, lignins, proteins and different flavanoids) demonstrates the piezoelectricity due to the rotation of the polar atomic groups or the formation of new dipoles upon the application of stress [48, 228]. The hydroxyl (–OH) groups in cellulose can interconnect the molecules through inter- and intra-molecular hydrogen bonding which develops the electric dipoles inside the crystal and, thereby, favors the induced crystallization of PVDF matrix to electroactive phase at the edges of the peel fiber as shown in the scheme of **Figure 6.8c** [81]. The piezoelectric effect is due to the displacement or reorientation of the dipoles in the crystal upon the application of stress [159, 229]. The long-range ordered polymer crystals undergo stress induces polarization causing the piezoelectricity under the mechanical stress. Although, the origin of piezoelectricity in the biomaterials is not clear yet as they do not follow the classical model of piezoelectricity, based on ideal crystalline structure [230]; however, the better piezoelectricity in the hybrid is due to electromechanical coupling arising from better interaction between the two phases under the application of pressure [212]. The working principle of the device under

compressed and release mode is explained in **Chapter 4**. The harvesting ability of the device is also verified with different human activities like bending (**Figure 6.10c)** and twisting **(Figure 6.10d)** and walking **(Figure 6.10e)**, which show output voltages of 5, 4 and 9 V, respectively, demonstrating the capacity of the device to generate power from normal body movements which otherwise go waste. A capacitor has been deployed to store the electricity generated by the hybrid generator and is able to be charged up to 1.2 V in 40 sec using finger tapping method and release the stored charge in another 40 sec time (**Figure 6.10f**). Another demonstration of LED lightening has been performed from the household door sliding using the hybrid generator to understand the efficacy of the hybrid device using bio-waste (**Figure 6.10g**). In gist, common bio-waste has been utilized to prepare hybrid material for energy generation by fabricating suitable device focusing the underlying mechanism of piezoelectricity arising from synergistic effect. Body movements and other waste mechanical energy like door sliding can efficiently be harvested through this hybrid device.

Part-3

6.4. PVDF hybrid with Pomegranate Peel

In this study we are using bio-waste pomegranate peel for piezoelectric energy harvesting. The pomegranate peel is used with Poly(vinylidene fluoride) to form a hybrid. There are some studies, which have shown that the pomegranate peel have antibacterial activity [231, 232], is antioxidant [233] and are used in different other ways [234, 235]. As best of our knowledge there is no study related to the waste peel generating usable electrical energy. This waste is a by-product of juice and syrup industries or its consumption as fresh fruit [234, 236]. The peel amount is almost 60 weight % of the fruit [237]. The proximate composition of pomegranate peel powder is shown in **Table 6.2**.

Table 6.2: Proximate composition of pomegranate peel powder [238].

Proximate Analysis	Results
Moisture	04±0.22(%)
Ash	05±0.14(%)
Fat	9.4±0.1(%)
pH	3.75±0.2
TSS	0.7±0.04(%)
Acidity	4.86±0.5(%)
Crude fiber	21±0.6(%)
Total sugar	31.38±0.3(%)
Reducing sugar	30.40±0.11(%)
Non-reducing sugar	0.98±0.12(%)
Nitrogen	1.395±0.30(%)
Protein	8.719±0.10(%)

6.4.1. Experimental:

Firstly, the pomegranate is peeled and its edible part and peels are separated. The peels are then dried and crushed to the powder. The PVDF and pomegranate peel is weighed according

to their weight percentage. We prepared 10, 20 and 40% of pomegranate peel powder (PM) content of hybrids. The hybrids were prepared by solution route as explained in **chapter 2**. The hybrids with 10, 20 and 30% of PM content are labeled as P-PM-10, P-PM-20 and P-PM-40.

Preparation of device for energy harvesting is explained in **Chapter 2**.

6.4.2. Results and Discussion:

6.4.2.1. Structure and morphology:

The pomegranate, its peel and the prepared hybrid is shown in **Figure 6.11a**. We can see that the hybrid is flexible enough and it is necessary to sustain the impact load on the device prepared by this hybrid. The X-ray diffraction pattern of pomegranate peel powder is shown in inset of **Figure 6.11b**, which shows its semicrystalline nature. **Figure 6.11b** shows the XRD pattern for the pure PVDF and PVDF-pomegranate peel powder hybrid. Pure PVDF has its characteristic peaks at 17.6°, 18.3° and 19.9° due to presence of α-phase [98, 203] , while in the hybrid we can see the absence of 17.6° peak, the peak at 18.3° shifts to 18.6° and the 19.9° peak shifts to 20.2° due to phase change from α to β and γ [99, 154]. Both β and γ-phases are piezoelectric in nature. PM induces β and γ-phase in PVDF through crystallization. The total piezoelectric phase in hybrid is calculated by XRD deconvolution and found to be ~55 %. The FTIR spectrum of PM is shown in **Figure 6.11c**, which shows the presence of alcohols, alkenes, ethers, alkenes and amides. The peak at 1730 and 1621 cm-1 shows the stretching vibrations of C=O and C=C, respectively. Peaks at 2935 and 2815 cm-1 shows the asymmetric and symmetric C-H stretching frequencies [239, 240]. The major functional groups present are indicated in the FTIR spectra of pomegranate peel powder. The

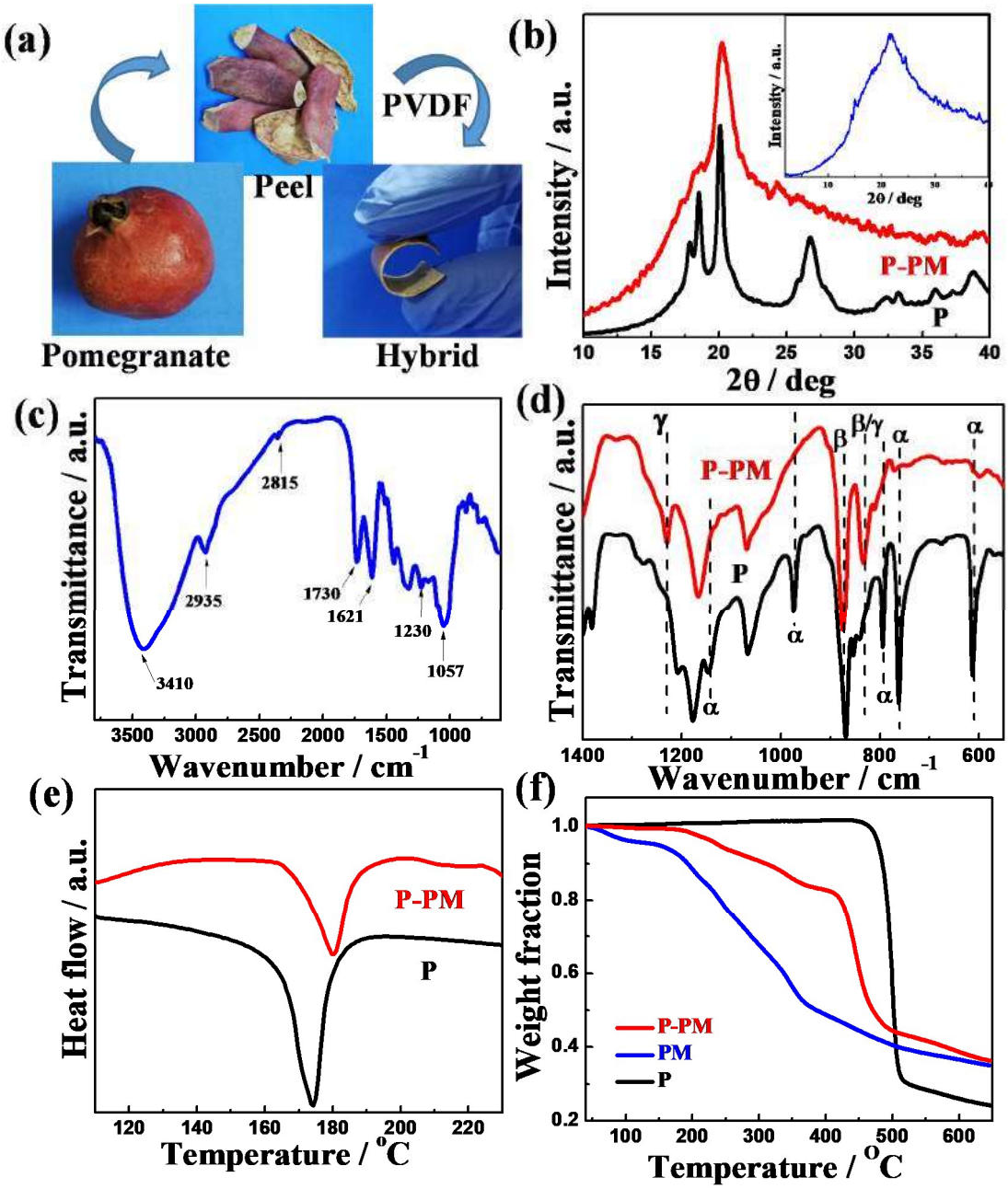

Figure 6.11: (a) Photographic image of Pomegranate, peel and its hybrid with PVDF (b) X-ray diffraction pattern of pure PVDF and hybrid (P-PM-40), inset shows the XRD of pomegranate peel (c) FTIR of pomegranate peel (d) FTIR of pure PVDF and hybrid (e) DSC of PVDF and hybrid, (f) Thermogravimetric analysis of for pure PVD, hybrid and pomegranate peel powder. (Here hybrid with 40% filler taken for comparison).

induction of both the piezoelectric phases (β & γ) and the decrease in α-phase can also be seen from the FTIR plot of hybrid (**Figure 6.11d**). The pure PVDF in its α-phase shows the peaks at 610, 760, 795, 972 and 1144 cm^{-1} [98, 203]. While the hybrid which have piezoelectric β and γ-phases shows peaks at 840, 878 and 1232 cm^{-1}, out of which the peak at 840 cm^{-1} is the combined peak of β and γ-phase [99, 226]. The peak at 878 cm^{-1} is the distinctive peak for β-phase and similarly the peak at 1232 cm^{-1} is the peak for distinctive γ-phase [99, 180]. The melting behavior of both pure PVDF and the hybrid is also studied by differential scanning calorimetry (**Figure 6.11e**). The pure PVDF has a melting temperature of 177°C, which increases in the hybrid to 182°C due to presence of γ-phase. The order of melting temperature of PVDF phases are γ>α>β [99, 154]. The thermal degradation behavior of the pure PVDF, hybrid and peel is shown in **Figure 6.11f**, which shows the thermal decomposition behavior of the hybrid. TGA plot for pomegranate peel powder shows that there are three main losses during the degradation of the PM. The first loss is between starting temperature and 160°C, which is attributed to moisture evaporation [241] and extractives [242]. The second loss ranging 160 to 370°C is due to decomposition of cellulose and hemicellulose [243]. And the third loss from 370 to 600°C can be the lignin degradation [242]. Moreover, it is reported [241] that the thermal decomposition of the organic matter occurs in the temperature range of 200-600 °C.

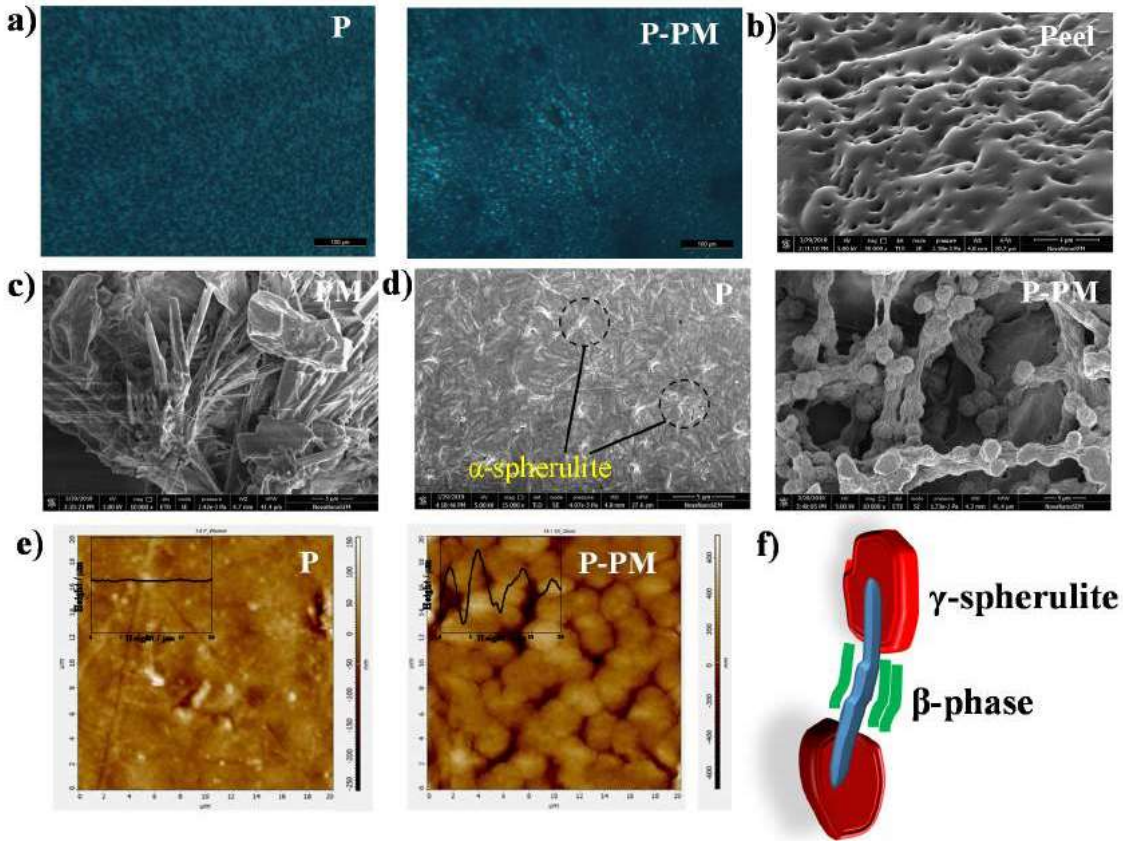

Figure 6.12: (a) POM images of pure PVDF and hybrid (b) SEM images of pomegranate peel and (c) peel powder and (d) PVDF and hybrid (e) AFM images of pure PVDF and hybrid, inset shows corresponding height profiles (f) schematic of crystallization of PVDF on peel fibers.

The changes in structure can also be described from the changes in the surface morphology. **Figure 6.12a** shows the polarized optical microscopy images of the pure PVDF and the hybrid. The pure PVDF has α-phase and the γ-phase in hybrid can be proved by the presence of the brighter spherulites. **Figure 6.12b, c** shows the scanning electron microscopy images of peel and peel powder, which clearly shows its fibrous and porous morphology. **Figure 6.12d** shows the SEM images of pure PVDF and hybrid; pure PVDF shows the spherulite pattern in the SEM images [99, 203] which is highlighted in the dotted circles. The hybrid shows the globules like morphology at the end of the fibers or whiskers of Pomegranate powder (PM), which might be formed due to crystallization of PVDF in the γ-phase. The β-

phase is present mostly in the vicinity of the whiskers. The atomic force microscopy images of pure PVDF and the hybrid is shown in **Figure 6.12e**, which shows similar structure as shown in the SEM morphology. The average height profiles of both are shown in the inset. The PVDF crystallizes in β and γ-phase (mostly γ) at the ends of the peel fibers as shown in **Figure 6.12f.**

6.4.2.2. Energy Harvesting:

The energy harvesting capability of the material is evaluated by preparing the device as explained in experimental section. The prepared piezoelectric device is able to generate voltage on application of mechanical stress. We prepared devices from pure PVDF, the hybrids with different filler content. The open circuit voltages from different devices are shown in **Figure 6.13a**. We can see that there is increase in the output voltage with the filler content, which shows the effect of filler in the piezoelectric hybrid. The device with highest filler percentage produces 65 V open circuit voltage as compared to only 6 V of pure PVDF. The corresponding power density (P) is calculated by measuring the output voltage across external resistances from

$$P = \frac{V^2}{R \times A}$$

where, V is output voltage, R is external resistance and A is the area of the device.

The maximum power density obtained from P-PM40 is 84 μW/cm^2 (**Figure 6.13b**). We also measured the power density of the device prepared from pure pomegranate peel, which is only 15 μW/cm^2. The less power density may be due to poor electrode attachment due to the rough surface of the peel. On the other hand the prepared hybrid shows high power density, this may be attributed to the synergistic effect of the filler with PVDF.

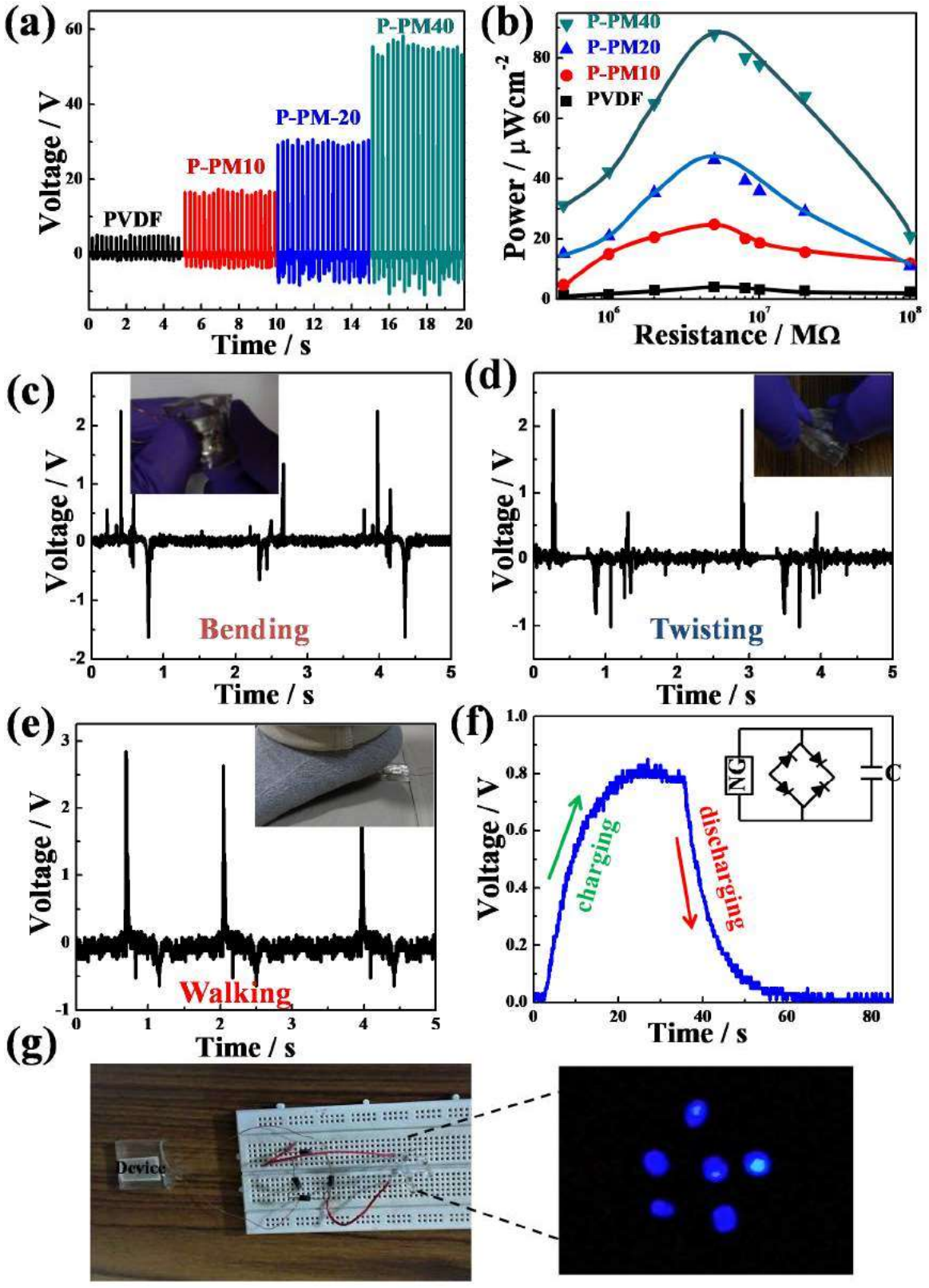
(a)
Voltage / V
Time / s
PVDF
P-PM10
P-PM-20
P-PM40
(b)
Power / μWcm-2
Resistance / MΩ
P-PM40
P-PM20
P-PM10
PVDF
(c)
Voltage / V
Time / s
Bending
(d)
Voltage / V
Time / s
Twisting
(e)
Voltage / V
Time / s
Walking
(f)
Voltage / V
Time / s
charging
discharging
NG
C
(g)
Device

Figure 6.13: (a) Open circuit voltage and (b) corresponding power density of pure PVDF and hybrids with different filler contents. Open circuit voltage on (c) bending, (d) twisting and (e) walking (f) capacitor charging on finger tapping and (g) LED lightening and corresponding circuit.

The working principle of the nanogenerator is explained in **Chapter 4**, which shows the generation of positive and negative charges on the surface of the device. The bio-waste (pomegranate peel composed of many proteins, sugars, fibers and acids) demonstrates the piezoelectricity due to the rotation of the polar atomic groups or the formation of new dipoles upon the application of stress [48, 228]. The hydroxyl (–OH) groups can interconnect the molecules through inter- and intra-molecular hydrogen bonding which develops the electric dipoles inside the crystal and, thereby, favors the induced crystallization of PVDF matrix to electroactive phase at the edges of the peel fiber as shown in the scheme of **Figure 6.12f** [81]. The piezoelectric effect is due to the displacement or reorientation of the dipoles in the crystal upon the application of stress [159, 229]. The long-range ordered polymer crystals undergo stress induces polarization causing the piezoelectricity under the mechanical stress. Although, the origin of piezoelectricity in the biomaterials is not clear yet as they do not follow the classical model of piezoelectricity, based on ideal crystalline structure [230]; however, the better piezoelectricity in the hybrid is due to electromechanical coupling arising from better interaction between the two phases under the application of stress [212]. The device is also able to produce voltage under various stresses, which shows the practical application of the device. Open circuit voltage under bending, twisting and walking is 3.8, 3 and 4 V respectively as shown in **Figure 6.13c-e**. The capacitor charging from the device by finger imparting is shown in **Figure 6.13f**. The capacitor is charged in almost 35 seconds and discharged in 30 seconds. The stored charge in capacitor can be used to power small devices.

Figure 6.13g shows the lightening of the LEDs by only finger imparting and corresponding circuit.

6.5. Conclusion:

This work demonstrates abundantly available bio-waste eggshell membrane, Orange peel and Pomegranate peel based PVDF hybrid nanogenerator as an efficient energy harvester. The prepared hybrids are sufficiently flexible and mechanically stable to sustain the stress applied from different types of body movements and common household activity. The eggshell membrane does not alter the structure of PVDF while nanoclay in presence of ESM almost completely converts the matrix polymer into piezoelectric phase. Orange peel induces the electroactive phases (β and γ) in matrix PVDF which eventually enhances the extent of piezo-phase (~70%) in the hybrid. Pomegranate peel also induces piezoelectric phase (β and γ) in the PVDF matrix. The structural conversion is confirmed through XRD and FTIR studies and is also supported by the morphological studies using optical and scanning electron microscope. Devices has been fabricated using these hybrids for energy harvesting. The device prepared with nanohybrid of PVDF-ESM and nanoclay shows a maximum power density of 55 $\mu W/cm^2$, while those of with orange and pomegranate peel shows power density of 135 and 84 $\mu W/cm^2$, under finger tapping. The devices are able to generate voltage under different types of mechanical stress and human body movements like bending, twisting, foot tapping, walking and common household activities, which shows its sensitive nature towards minimal load with significantly high power output. The devices are capable of charging the capacitor and lightening the LEDs with different kind of stresses. Thus, we can say that these bio-waste based hybrids are promising material for the energy harvesting and as an alternative green energy source for powering small electronic devices in real life applications.